Zhou, J., Zhang, Y., **Balda, M.**, Presser, V., **Kopinke, F.-D.**, **Georgi, A.** (2022):
Electro-assisted removal of polar and ionic organic compounds from water using activated carbon felts
Chem. Eng. J. **433** (Part 2), art. 133544

http://dx.doi.org/10.1016/j.cej.2021.133544

Electro-assisted removal of polar and ionic organic compounds from water using activated carbon felts

Jieying Zhou[a], Yuan Zhang[b,c], Maria Balda[a], Volker Presser[b,c,d],
Frank-Dieter Kopinke[a], Anett Georgi[a]*

[a] *Helmholtz Centre for Environmental Research – UFZ, Department of Environmental Engineering, 04318 Leipzig, Germany*
[b] *INM - Leibniz Institute for New Materials, 66123 Saarbrücken, Germany*
[c] *Department of Materials Science and Engineering, Saarland University, 66123 Saarbrücken, Germany*
[d] *saarene, Saarland Center for Energy Materials and Sustainability, Campus C4 2, 66123 Saarbrücken, Germany*
* *Corresponding author contact information: E-mail: anett.georgi@ufz.de*

Keywords:

electrosorption; activated carbon; surface modification; polar organic micropollutant; ionic organic micropollutant

Abstract

Highly water-soluble, persistent, and mobile organic compounds (PMOCs) are more and more often detected in surface and groundwater, evoking potential threats to the environment and human health. Traditional water treatment strategies, including adsorption by activated carbon materials, fail to efficiently remove PMOCs due to their hydrophilic nature. Electro-assisted sorption processes offer a clean, facile, and promising solution to remove PMOCs on activated carbon-based electrodes and potentially allow an easy on-site sorbent regeneration (trap&release). In this work, the electrosorption of five selected PMOCs, that is, tetrapropylammonium (TPA^+), benzyltrimethylammonium ($BTMA^+$), *p*-tosylate (*p*-TsO^-), *p*-toluenesulfonamide (*p*-TSA), and methyl-*tert*-butyl ether (MTBE), were investigated on two comprehensively characterized activated carbon felt (ACF) types carrying different surface functionalities. Significant enrichment factors in ranges of 10^2 to 10^3 for charged PMOCs were expected by our first estimation for electro-assisted trap&release on ACFs in flow systems applying potentials in the range of -0.1 V/+0.6 V vs. SHE for ad-/desorption, respectively. Defunctionalized ACF carrying larger density in surface π-systems and lower O-content promises a higher capability in electrosorption processes than the pristine material in terms of better material stability (tested for 5 cycles over 500 h) and better removal efficiency of ionic PMOCs. To improve ACFs adsorption performance for cationic and anionic PMOCs, permanent chemical surface modification and reversible electric polarization as alternative strategies are compared. Our findings explore future electrode and process design of electrosorption for applications to treat water contaminated by emerging PMOCs.

1. Introduction

Diverse organic compounds are contained in industrial and domestic wastes, which cause water pollution. While most persistent organic pollutants (POPs) regulated in the Stockholm Convention [1] are inherently not well water-soluble, a considerable proportion of emerging organic contaminants are identified to have highly polar, ionizable, or ionic structures [2, 3]. They form the group of persistent and mobile organic compounds (PMOCs) [2, 4]. Although modern wastewater treatment plants (WWTPs) can effectively remove many non-polar organic compounds, PMOCs may slip through the conventional technical barriers, exposing a treatment gap for drinking water [4] and potential threats to human health [5-8].

Existing typically in low concentrations (ng/L to mg/L) [9], PMOCs need to be pre-enriched before any degradation approaches for an energy-efficient and cost-effective treatment. Adsorption using activated carbon (AC) with a high specific surface area ($\geq 10^3$ m^2/g) is presently the prevailing technique to enrich organic micropollutants on adsorbents from wastewater in WWTPs [4, 10]. The less satisfying adsorption efficiency of AC-based materials to highly polar PMOCs can be enhanced by tailoring sorbent surface chemistry [11-14] or electrically polarizing conductive sorbent surfaces [15-17]. By tuning the electric field in the latter approach, desorption conditions can be met to regenerate exhausted adsorbents *in-situ* [15-19]. This may promote a green alternative for the state-of-the-art AC regeneration strategy: off-site high-temperature treatment associated with substantial carbon loss and CO_2 release, extra transportation burden, and considerable negative environmental impact [20]. On-site adsorbent regeneration using renewable electric energy is even more appealing for treating highly mobile PMOCs where early adsorber breakthroughs occur and short regeneration intervals are required accordingly.

The last decade has seen vast development in water desalination especially via capacitive deionization (CDI) where electrosorption processes on AC-based materials find their major application so far [21, 22]. With the increased awareness of PMOC pollution in water and the call for on-site adsorbent regeneration, research interest gradually arises in the electrosorption of polar organic compounds. Ionizable/ionic organic compounds, partially highly environmentally relevant, were selected as target adsorbates in a few studies published during the past two decades [15-17, 23-35]. For instance, Wang *et al.* [29] revealed a 5-fold higher adsorption capacity to the ionizable antibiotics sulfadimethoxine, ciprofloxacin and clarithromycin in a two-electrode flow unit equipped with AC felts upon mild polarization (cell voltage = 1.0 V). Still, compared to the achievements in the field of CDI, electrosorptive approaches for efficient removal of PMOCs remain to be established where an in-depth understanding of electrosorption behaviors of various PMOCs is essential. Nevertheless, very little work has covered PMOCs with nonionic, cationic, and/or anionic structures [29, 34, 36] as we present here.

Since the concept of electro-assisted ad-/desorption, described here as trap&release approach, was first introduced in 1986 by Woodard *et al.* [36] to remove Rhodamine B using three-dimensional carbon fibers, it has been so far only explored by a few studies for limited polar, ionizable/ionic organic compounds [15, 17-19, 24, 29, 34, 37]. Our recent work [15] estimated achievable enrichment factors, that is, the ratio of water volume cleaned in the electro-adsorption step to the volume needed for electro-desorption, to be in the range of 40 to 100 for perfluoroalkyl acids (PFAAs) using AC carrying different surface functionalities. This suggests the great potential of electro-assisted trap&release in PMOC removal which shall be investigated for a broader selection of various candidates. In addition, AC adsorbents with modified surface chemistry were not involved in the past research except in our previous study [15], leaving it unsolved how AC surface chemistry would improve or inhibit its electro-ad-/desorption efficiency towards a variety of PMOCs. Moreover, except for a few cases [18, 19, 38], investigation of adsorbent stability during the electro-assisted trap&release process was generally missing to provide valuable insight into system long-term stability.

To identify the drivers for an effective, long-term stable electrosorptive removal of PMOCs from water, pristine and surface-defunctionalized activated carbon felts (ACFs) were polarized at different bias potentials to ad-/desorb five PMOCs, that are tetrapropylammonium (TPA^+), benzyltrimethylammonium ($BTMA^+$), *p*-toluenesulfonate (*p*-TsO^-, $pK_{a,p\text{-}TsOH} < -1$ [39, 40]), *p*-toluenesulfonamide (*p*-TSA, $pK_{a,p\text{-}TSA} = 10.5$ [41]), and methyl-*tert*-butyl ether (MTBE). This selection covers two cationic, one anionic, and two nonionic (at neutral pH), highly environmentally relevant PMOCs detectable in various aquatic environments [2, 9, 42]. These PMOCs were found in ng/L - µg/L range in various surface waters worldwide [9, 43, 44] while the concentration in wastewater can be in the range of µg/L – mg/L [43, 45] (detailed pollution levels see **Table S1**). Their electrosorption behaviors on AC materials are investigated here for the first time.

In addition to charging AC adsorbents via an externally applied electric potential, chemical modification can alter the native charge state of an AC surface in a specific aqueous environment. The latter is related to protonation/deprotonation equilibria, which can also be decisive in the adsorption of ionic and polar PMOCs without any external electric potential [13]. Surface polarization via applied bias potential and surface chemical modification can both be employed to generate differently charged AC surfaces to influence PMOC adsorption; yet, works in the past have explored them in individual studies and not in a much-needed comparative approach. Here, we applied both approaches in case studies of cationic TPA^+, anionic *p*-TsO^-, and nonionic *p*-TSA adsorption on ACFs and compared their effects for the first time. Adsorption isotherms determined in batch systems were fitted with Freundlich and Langmuir equations to quantify the adsorption capacity and affinity of differently surface-functionalized ACFs towards various PMOCs under selected polarization conditions.

We also evaluated the applicability of the electro-assisted trap&release approach using two ACFs. To this end, we analyzed 1) the impact of applied bias potential on single-point sorption coefficients K_d in batch systems for different PMOCs, and 2) the estimated achievable enrichment factors in a fixed-bed flow-through setup derived from Freundlich isotherm parameters collected under electro-ad-/desorption conditions in batch systems for the most promising PMOC candidates. The system stability was examined by ad-/desorption cycles of TPA^+ and p-TsO^- on surface-defunctionalized ACF over 20 d, where potential changes in adsorbent properties were monitored via cyclic voltammetry (CV), temperature-programmed decomposition (TPD), and determination of the pore structure.

2. Experimental Section

2.1 Chemicals

BTMA-OH (20 wt% aq.) and p-$TsOH \cdot H_2O$ (>98.5%) were purchased from Alfa Aesar. TPA-OH (1 M, aq.) and *p*-TSA (≥99%) were obtained from Sigma-Aldrich. MTBE (>99%) was purchased from Fluka Analytical. Selected sorbate properties are listed in **Table 1**. Na_2SO_4 (99%), NaOH (99%), HCl (37%), $NaNO_3$ (>99%), KCl (>99%), H_2SO_4 (0.5 M) and HNO_3 (65%) were purchased from Merck. Methanol (>99.95%) and 2-propanol (≥99.9%) were purchased from Th. Geyer. Ammonium acetate ($C_2H_7NO_2$, ≥98.0%) was obtained from Bernd Kraft GmbH. All solutions were prepared using deionized water.

2.2 Materials

Actitex-FC1001 (Jacobi CARBONS; referred to as ACF_{10} in short in the following text) was pre-treated and further modified according to the procedures reported previously [13] to be tested for PMOC adsorption with and without electrical polarization. As a modification, we applied less hazardous H_2/N_2 (forming gas) instead of pure H_2 flow for surface defunctionalization to remove various oxygen-containing groups. In short, the sample was washed once with 2-propanol and 5 times with H_2O under shaking (each 30 min, 120 rpm) and then dried in air overnight (16 h) at 80°C before being ready for use. Surface defunctionalized ACF ($DeACF_{10}$) was generated by heating ACF_{10} in a tubular quartz oven (length: 40 cm, Ø: 2 cm) from room temperature to 900°C in a H_2/N_2 1:10 mixture (150°C/min, 40 mL/min gas flow) and kept at 900°C for 2 h. The oven with the sample inside was purged before heating with N_2 flow for 0.5 h, followed by adding H_2 gas and purging for another 10 min. After the heating procedure, the H_2 flow was kept until the oven had cooled below 500°C. The sample was continued to cool down in N_2 flow until $T < 100°C$ before being taken out. It was then washed 5 times with water (30 min each, 120 rpm shaking) and dried overnight at 80°C before characterization. Note that the samples defunctionalized in the H_2/N_2 mixture exhibited nearly identical characteristics compared to the sample prepared in the pure H_2 flow. Oxidized ACF ($OxACF_{10}$) was accomplished by treating ACF_{10} (1.0 g) in 5 M HNO_3 (120 mL) for 6 h at 95°C to introduce more oxygen-containing groups including carboxylic, carbonyl, and hydroxyl groups on the carbon surface [13]. After washing with H_2O for 5 times (each 30 min, 120 rpm) until the solution pH approached 6, the sample was dried in air overnight at 50°C before further usage.

2.3 Material characterization

The pore size distributions and specific surface areas (SSA) were measured by applying an Autosorb iQ system under the N_2 atmosphere at -196°C. The quenched solid density functional theory (QSDFT) was applied for analysis by assuming a slit-shaped pore configuration. The electrode sample was first degassed at 100 Pa and 200°C for 1 h and then heated to 300°C for 20 h.

Raman spectroscopy was performed by a Renishaw inVia Raman spectrometer equipped with a 532 nm Nd-YAG laser (exposed power 0.5 mW on the sample, 2400 lines/mm grating, 50x objective with 0.75 numeric aperture). For each ACF sample, 10 points were selected to be measured. An acquisition with 5 accumulations was applied for each measurement point. Peak deconvolution was performed using a linear background and Voigt profiles for the fitting.

The point of zero net proton charge (pH_{PZC}) of the ACFs was determined based on the procedures in [46]. In brief, a 10 mg sample was stirred overnight in 2 mL of aqueous 10 mM Na_2SO_4 electrolyte solution at various initial pH values (2-11) adjusted using 0.1 M NaOH and 0.05 M H_2SO_4 solutions. The pH values were recorded before and after. The pH_{pzc} of the sample is the point where pH (initial) = pH (final).

Scanning electron microscopy was conducted to observe the morphology of the materials. A Zeiss Gemini SEM 500 is applied with a working distance of ca. 5 mm. The applied power for observing the samples is 1 kV. The samples were sticked on copper tape without sputtering coatings.

Temperature-programmed decomposition (TPD) measurements were performed with a BELCAT-B chemisorption analyzer (BEL) connected to an IR detector (SAXON Junkalor). The samples were kept first in Ar at 150°C for 30 min before being heated up to 1100°C in a He flow (50 mL/min, 10°C/min), and evolving CO and CO_2 gases were detected. Elemental analysis was done with a CHN analyzer (LECO TruSpec CHN). The ash content was measured gravimetrically as residue after sample combustion at 750°C in O_2.

Experimental details of attenuated total reflection (ATR)-FTIR and determination of anion and cation exchange capacities (AEC and CEC) are described in the *Supporting Information*.

Cyclic voltammetry (CV) was carried out using a multi-channel potentiostat MSX-8 (ScioSpec). A three-electrode cell consisting of a Pt helix counter electrode, an Ag/AgCl sat. KCl reference electrode and a working electrode made of a piece of ACF (connected with a Pt wire) or a graphite rod, or a piece of boron-doped diamond (BDD) was used for the measurement. 1 M or 10 mM Na_2SO_4 aqueous solution (initial pH 6.8-7.0) was used as the electrolyte background solution. Before measurements, the solution was bubbled with N_2 under stirring (300 rpm) for 15 min to remove the dissolved O_2. During the measurement, the upper gas phase of the cell was continuously purged with N_2. All reported potential values were converted to potential vs. the standard hydrogen electrode (SHE) unless expressly stated (E ([V] vs. SHE) = E ([V] vs. Ag/AgCl sat. KCl) + 0.20 [V]).

Electrochemical impedance spectroscopy (EIS) measurements were performed using a specially designed cell carrying a poly(ether ether ketone) body (PEEK, outlined in Ref. [47]) and recorded by a BioLogic potentiostat (VMP-300). The PEEK cell is equipped with an Ag/AgCl sat. KCl reference electrode, an oversized YP-80F (Kuraray) activated carbon mixed with 10 wt% poly(tetrafluoroethylene) binder, and a working electrode made of ca. 10 mg ACF. The detailed structure of the cell is described in [47]. 1 M Na_2SO_4 aqueous solution was used as the electrolyte background. Frequencies ω in the range of 3 mHz to 1 kHz and potentials, where the studied ACF can be regarded as ideal polarizable electrodes, were applied. In this potential range, the areal capacitance C (F/m^2) can be obtained from the impedance imaginary part Z_{Im} at any electrode potential via $C = -(\omega \cdot Z_{\mathrm{Im}})^{-1} / (m \cdot \mathrm{SSA})$ [48, 49], where m (g) is the sample mass and SSA (m^2/g) the specific surface area. To determine the potential of zero charge (E_{pzc}) of ACFs, data collected at frequencies where $Z_{Im} = f(\omega)$ can be used. Here we chose ω = 96.2 mHz at which Z_{Im} showed a clear dependence on ω in the nearby range. The potential where the areal capacitance reaches its minimum is assigned to be the ACF's E_{pzc}.

2.4 Adsorption experiments without applying external bias potential

Adsorption experiments without applying external potential on ACFs were performed according to the published protocols [13]. Briefly, the sorbent was pre-wetted in 10 mM Na_2SO_4 background solution assisted by shaking (120 rpm) for 1-2 d with pH adjustment to 7 using 0.05 M H_2SO_4 and/or 0.1 M NaOH solution. Then, aqueous stock solutions of sorbates, which were neutralized beforehand, were given to achieve various initial concentrations in the range of 2-100 mg/L (single compound batches). After 48 h of orbital shaking at 120 rpm with daily pH adjustment to 7, aliquots were taken through Whatman PTFE (0.45 µm) syringe filters for measurements. Examples of adsorption kinetics are given in *Supporting Information*, **Fig. S1**, indicating an approach to equilibrium within 48 h. The pH values of the background solutions were monitored to be within 7.0 ± 0.5 after adsorption.

2.5 Electrosorption experiments

Electrosorption experiments were performed in a three-electrode batch cell consisting of an ACF working electrode (connected with a Pt wire), an Ag/AgCl sat. KCl reference electrode and a Pt helix counter electrode, connecting to a multi-channel potentiostat MSX-8 (ScioSpec) (**Fig. S2**). An aqueous 10 mM Na_2SO_4 solution (initial pH 6.8-7.0) was used as background electrolyte solution with ACF dosage kept at 1 g/L. A $DeACF_{10}$ dosage of 0.25 g/L was used for systems containing *p*-TSA. ACF was pre-wetted in stirred (300 rpm) solution overnight before adjusting pH using 0.1 M NaOH and 0.05 M H_2SO_4 to 7.0 ± 0.3. Then, the open circuit potential

(OCP) of ACF was measured by a multimeter. The system was purged with N_2 (water-saturated) for 15 min before charging the ACF at desired potentials. After 24 h polarization, the electrolyte solution was again adjusted to neutral pH before stock solutions containing target compounds were added to achieve initial concentrations in the range of 2-300 mg/L under N_2 purging. For cells containing MTBE, the purging step was skipped. A second pH adjustment step was carried out for cells containing TPA^+, $BTMA^+$, *p*-TsO^- or *p*-TSA at 24 h after adding the stock solutions. For measurement, samples were taken 48 h after stock solution addition through Whatman PTFE (0.45 µm) syringe filters. Also, in cycle experiments, each ad-/desorption step lasted 48 h to ensure the approach to sorption equilibria. Adjusting pH to 7.0 ± 0.3 was performed daily while N_2 purging was kept throughout the experiment (5 cycles for 20 d in total).

2.6 Analytical methods

The aqueous samples were analyzed with methods reported previously [13]. In short, analysis of samples containing *p*-TsO^- was done by HPLC (LC-SPD-M20A, SHIMADZU) coupled with a UV/VIS detector at λ = 220 nm. Samples containing TPA^+ were analyzed with HPLC-MS (LCMS-2020, SHIMADZU) in SIM mode (m/z = 186 amu). $BTMA^+$ and *p*-TSA were analyzed by UV/VIS (UVmini-1240, SHIMADZU) at λ = 207 nm and 225 nm, respectively. MTBE was measured using Headspace-GC-MS (GCMS-2010, SHIMADZU).

2.7 Sorption calculations

The adsorption affinity of ACFs was indicated by the single point adsorption coefficient K_d (L/m^2) at the adsorption equilibrium according to **Eq. 1**:

$$K_\mathrm{d} = \frac{q_\mathrm{e}}{c_\mathrm{e}} \tag{1}$$

where the loading on the sorbent is given by q_e (µmol/m^2), and the sorbate equilibrium concentration in the water phase is given by c_e (µmol/L).

To analyze the adsorption isotherms, Freundlich (**Eq. 2**) and Langmuir fittings (**Eq. 3**) were employed:

$$\log q_\mathrm{e} = n \cdot \log c_\mathrm{e} + \log K_\mathrm{F} \tag{2}$$

$$\frac{c_\mathrm{e}}{q_\mathrm{e}} = \frac{c_\mathrm{e}}{q_\mathrm{m}} + \frac{1}{q_\mathrm{m} K_\mathrm{L}} \tag{3}$$

The Freundlich parameters include n as the dimensionless Freundlich exponent and K_F in (µmol/m^2)/(µmol/L)$^\mathrm{n}$ as the Freundlich constant. The Langmuir parameters include q_m (µmol/m^2) as the maximal sorbent loading (only monolayer adsorption considered) and K_L (L/µmol) as the so-called Langmuir constant. The adsorption affinity of the sorbent is indicated by K_F and K_L values, while the adsorption capacity is represented by q_m. Furthermore, n being close to 1 refers to relatively homogenous sorption sites and conditions far below maximum loading [14, 19].

In this work, we utilize the so-called trap&release strategy powered by switching the electro-assisted ad-/desorption steps to achieve I) enhanced removal of PMOCs and II) adsorbent regeneration. The trap&release performance can be estimated based on a fixed-bed flow-through model, which is closer to the reality than a batch design in wastewater treatment, using Freundlich n and K_F values derived from batch adsorption experiments [29]. Through an effective trap&release process, the water volume needed for desorbing the contaminants (V_des) shall be significantly reduced compared to the volume of treated inflow water (V_ads with contaminant concentration c_in). The concentrate obtained by electrodesorption can then be used for further degradation or treatment approaches. The extent of adsorbent unloading (X_des) is defined by **Eq. 4**:

$$X_\mathrm{des} = 1 - \frac{q_\mathrm{des,final}}{q_\mathrm{ads}} \tag{4}$$

with q_{ads} as loading achieved in the adsorption step and $q_{\mathrm{des,final}}$ as loading remaining after the desorption step. When using clean water for desorption, 100% adsorbent unloading is expected. In this case, the enrichment factor, i.e., $V_{\mathrm{ads}}/V_{\mathrm{des}}$ achieved by the trap&release strategy, can be estimated according to **Eq. 5**; see *Supporting Information* for the derivation.

$$\frac{V_{\mathrm{ads}}}{V_{\mathrm{des}}} = c_{\mathrm{in}}^{(n_{\mathrm{ads}}/n_{\mathrm{des}}-1)} \cdot \left(\frac{K_{\mathrm{F,ads}}}{K_{\mathrm{F,des}}}\right)^{1/n_{\mathrm{des}}} \tag{5}$$

Alternatively, when using inflow water (i.e., the water to be treated by electrosorption) directly for desorption, the ratio of $V_{\mathrm{ads}}/V_{\mathrm{des}}$ can be calculated according to **Eq. 6-7** [15]:

$$\frac{V_{\mathrm{ads}}}{V_{\mathrm{des}}} = \frac{c_{\mathrm{in}}^{(n_{\mathrm{ads}}/n_{\mathrm{des}}-1)} \cdot \left(\frac{K_{\mathrm{F,ads}}}{K_{\mathrm{F,des}}}\right)^{1/n_{\mathrm{des}}} - 1}{X_{\mathrm{des}}} \tag{6}$$

$$\text{with } X_{\mathrm{des}} = 1 - \frac{K_{\mathrm{F,des}}}{K_{\mathrm{F,ads}}} \cdot c_{\mathrm{in}}^{(n_{\mathrm{des}}-n_{\mathrm{ads}})} \tag{7}$$

3. Results and Discussion

3.1 Characterization results of ACFs

The chemical properties of ACF_{10} and $DeACF_{10}$ characterized using elemental analysis, pH_{PZC}, ion exchange capacity measurement, TPD, and XPS were described in detail previously [13]. Selected results are summarized in *Supporting Information*, **Table S2**. Raman spectra are shown in **Fig. S3**. The textural properties of ACFs are provided in **Table S3** and **Fig. S4**, and FT-IR spectra are shown in **Fig. S5**. The data demonstrate that both ACFs are predominantly microporous with a volume-weighted, average pore diameter of ca. 1 nm. ACF_{10} (O/C = 0.11 by mass) is richer in O-content than $DeACF_{10}$ (O/C = 0.05 by mass) according to the elemental analysis results. ACF_{10} is negatively charged and more abundant in cation exchange sites at circum-neutral pH with a pH_{PZC} ~ 6.0. In contrast, $DeACF_{10}$ (pH_{PZC} ~ 10.0) carries a positively charged surface at circum-neutral pH via the adsorption of protons from the aqueous environment onto its delocalized π-electron systems [11]. The significant amount of

sp^2-hybridized carbon of $DeACF_{10}$ surface is confirmed by XPS analysis [13] and Raman results (**Fig. S3**), pointing to a higher surface hydrophobicity than ACF_{10}.

Herein, the electrochemical properties of ACF_{10} and $DeACF_{10}$, being particularly important in terms of electro-assisted sorption processes, were characterized by CV and EIS, as shown in **Fig. 1-2**. Cyclic voltammograms were used to investigate the electrochemical processes at different potentials and to quantify the material's capacitance. For ACF_{10}, the oxidation current slightly increased above +0.7 V. This can be assigned to the oxidation of the carbon surface as the standard potential for carbon oxidation is reported at +0.21 V (at 25 °C, c_{H+} = 1 M, p_{CO2} = 101.3 kPa) [50], equivalent to ca. +0.65 V at neutral pH. The reduction current started to decline below +0.2 V, which might refer to the reduction of the remaining oxygen despite the N_2 purging (**Fig. S7**) or the reduction of the carbon surface (the respective standard potential so far not available) [50]. The electrochemically stable potential window of ACF_{10} (in short as ''potential window'' in the following text), in which no Faradaic reactions of the electrode occurs, is between +0.2 V and +0.7 V. This range is well consistent with the reported potential map of redox processes of microporous activated carbon cloths in the aqueous phase [51]. The CV curve of $DeACF_{10}$ in **Fig. 1a** shows neither a significant rise of the oxidation current below +0.6 V nor a decline of the reduction current beyond -0.1 V. Thus, the potential window of $DeACF_{10}$ is estimated to be between -0.1 V and +0.6 V, reflecting its lower surface oxidation degree than ACF_{10}. Information on the stability of ACFs at the edge of the potential windows can be found in *Section 3.4*. ACF_{10} shows a capacitance of 0.059-0.082 F/m^2 in the range of +0.2 V to +0.7 V normalized to its SSA, which is 100-139 F/g (**Fig. 1a**). $DeACF_{10}$ presents an areal capacitance of 0.070-0.083 F/m^2 in the range of -0.1 V to +0.6 V, which is 98-116 F/g normalized to its mass. For comparison, the CV result of $OxACF_{10}$ is shown in **Fig. S6**. A strong decline in specific capacitance (**Fig. S6a,b**) was clearly seen after surface oxidation, probably resulting from pore blocking by oxygen-containing functional groups [52, 53].

As seen for cyclic voltammograms obtained in 10 mM Na_2SO_4 at a scan rate of 0.5 mV/s (**Fig. 1b**), the narrowing of the CV oxidation and reduction branches visualizes a more obvious V-shape region compared to those obtained in 1 M Na_2SO_4 at a scan rate of 1 mV/s. Previous research suggested the electrode's E_{pzc}, that is, the potential at which the electrode surface carries a zero net charge, is linked to the V-shaped region [54]. They related the appearance of V-shapes to electrochemical doping [47] or overlapping of the electrochemical double-layer formation in microspores at low scan rates [55]. E_{pzc} of ACF_{10} is expected to fall within the region of +0.4 V to +0.7 V. The V-shape region is shifted to lower potential for $DeACF_{10}$, that is, from 0 V to +0.2 V, confirming its reduced character [54].

The EIS measurements of ACFs provided a more accurate determination of the material's E_{pzc}. **Fig. 2a** shows the change in areal capacitance C of ACFs at different applied potentials measured in 1 M Na_2SO_4 at pH = 7. The electrode's E_{pzc} is located at the potential showing a minimal C. E_{pzc} was proven to be adversely related to the material's pH_{pzc} [54]. Electric charges are needed to compensate the material's native surface charges (and repulse counterions) prevalent at the pH conditions until a zero net charge state at $E = E_{pzc}$ is reached. Thus, a significantly lower E_{pzc} is found for $DeACF_{10}$ compared to ACF_{10} ((0.20 ± 0.05) V and (0.40 ± 0.05) V, respectively) following its higher pH_{pzc} value (ca. 10.0 compared to 6.0 for ACF_{10}). $OxACF_{10}$ containing the highest surface O-content shows the lowest pH_{pzc} (**Table S2**) and accordingly the highest $E_{pzc} > 0.80$ V (**Fig. S6**). At $E > E_{pzc}$, the electrode surface becomes positively charged and accumulates SO_4^{2-} from the background Na_2SO_4 solution, whereas it is negatively charged at $E < E_{pzc}$ and preferentially takes up Na^+. The OCPs of ACF_{10} and $DeACF_{10}$ are both measured to be (0.45 ± 0.05) V in Na_2SO_4 solution at pH 7. This value indicates a nearly neutral surface of ACF_{10} while a strongly positively charged $DeACF_{10}$ surface in the absence of external potential. Anion exchange capacities reported previously for ACF_{10} (0.025 µmol/m^2) and $DeACF_{10}$ (0.23 µmol/m^2) measured at pH 7 [13] also confirm such charging status suggested by the material's E_{pzc}.

The derived Nyquist plots (**Fig. 2b**) show a characteristic intercept with the Z_{Re}-axis, standing for the total resistance of the electrodes and electrolytes [56, 57], and linear lines with angles below 45° at low frequencies, typical for electrical double-layer capacitors [48]. For ACF_{10}, a half semi-circle is visible before the transition to the 45°-range; this half semi-circle is absent for $DeACF_{10}$. Thereby, $DeACF_{10}$ behaves more like an ideal capacitor with less ion transport limitation imposed by micropores. $DeACF_{10}$ also shows a smaller charge transfer resistance, possibly owed to a better charge transfer at the electrode/current collector interface [58]. The Nyquist plot of $OxACF_{10}$ in **Fig. S6c** shows a longer 45° line compared with ACF_{10} and $DeACF_{10}$, which represents a more limited micropore accessibility and higher resistivity for ion diffusion in the pores under the applied potential.

3.2 Effect of bias potential on the adsorption of selected PMOCs

The electrosorption of selected PMOCs was investigated on ACF_{10} and $DeACF_{10}$ polarized at voltages within their potential windows. $OxACF_{10}$ was not involved as an option for an active electrosorption electrode due to its much smaller specific capacitance than ACF_{10} and $DeACF_{10}$. The selected PMOCs do not undergo electrochemical redox reactions under the probed conditions as indicated both experimentally in *Supporting Information*, **Fig. S7** and suggested in previous research [59, 60]. **Fig. 3** demonstrates the effect of electrode polarization on PMOC adsorption by showing the change in logarithmic single-point sorption coefficients K_{d} along with the applied potential.

As shown in **Fig. 3**, the nonionic adsorbates *p*-TSA and MTBE adsorption were only slightly affected by applying external potentials on ACFs. Only an insignificant increase in log K_d was observed at lower potentials. For the ionic PMOCs TPA$^+$, BTMA$^+$, and *p*-TsO$^-$, log K_d generally increased along with potential values in the opposite direction to the sorbate charge, indicating a promoted adsorption affinity caused by enhanced electrostatic attraction. In contrast, applying potentials in the same direction to the PMOCs' permanent charges led to a decrease in log K_d, where desorption processes are facilitated due to stronger electrostatic repulsion. K_d values differed by a factor larger than 5 on both ACFs for all probed ionic PMOCs at adsorption vs. desorption conditions, that is, the boundary potentials allowed by the electrode potential windows. We see promising PMOC removal efficiency and significant capability for on-site adsorbent regeneration utilizing an electro-assisted trap&release strategy from these values. Similar approaches showed satisfactory results previously for the removal of perfluoroalkyl acids [15]. DeACF$_{10}$ allows a wider potential window than ACF$_{10}$ where the sorbent remained electrochemically stable. Higher ratios in $K_{d,ads}/K_{d,des}$ on DeACF$_{10}$ for ad-/desorption processes (up to 159 for TPA$^+$ and 47 for *p*-TsO$^-$) can be achieved compared with 67 and 5 on the original ACF$_{10}$, respectively.

To further investigate the effect of electrode polarization on PMOC adsorption, we determined adsorption isotherms of TPA$^+$ and *p*-TsO$^-$ on the two ACF types (**Fig. 4**), both at OCP and selected ad-/desorption potentials. Derived from Freundlich parameters (**Table 2**, **Fig. S8**), we estimated achievable enrichment factors (V_{ads}/V_{des} ratios) in **Table 3** for the trap&release according to **Eq. 5-6** by assuming c_{in} = 100 μg/L for both TPA$^+$ and *p*-TsO$^-$ inflow water. The bias potential at which the highest K_d is delivered in **Fig. 3a-b** is set for the *trap* condition, while for the *release* steps the potential at which the lowest K_d is achieved. When using inflow water for desorption, around 90% adsorbent unloading is achievable in all trap&release cases. Using clean water for desorption (i.e., at 100% adsorbent unloading), an enrichment factor of 65 and 42 for TPA^+ and p-TsO^-, respectively, can be achieved by electro-assisted trap&release on ACF_{10}. These values increase to 780 and 158 on $DeACF_{10}$, indicating a much stronger polarization-induced effect. The ionic PMOCs could be enriched by factors of 10^2 to 10^3 by manipulating the electrosorption conditions on defunctionalized AC surfaces. This is more than 10-times the enrichment factor achievable using a typical reverse osmosis setup for treating wastewater containing PMOCs [4, 61], underlining the promising efficiency of electro-assisted trap&release. However, its performance needs to be carefully evaluated further in real applications. If a flow system is smartly designed employing a suitable ACF dosage, a large volume of water can be cleaned by multiple runs of electro-assisted trap&release procedures to pre-concentrate PMOCs ready for further treatment or degradation steps. In addition, our approach allows flexible choices of the water type used for desorption depending on factors such as economic considerations, water composition and requested emission limits of the relevant pollutants.

The isotherms in **Fig. 4** also illustrate the influence of applied potentials on ACFs' adsorption capacities towards TPA^+ and p-TsO^-. Langmuir fitting (**Eq. 3**) was applied to the isotherms as shown in **Fig. S9** to derive the adsorption capacities. Both adsorption affinities (K_d) and capacities (q_m) of the ACFs towards ionic PMOCs can be manipulated through electrode polarization. As shown in **Table 2**, compared to the q_m achieved under OCP conditions (+0.45 V), q_m of TPA^+ on ACF_{10} increases by 1.7 times at +0.2 V whereas decreases about by half at +0.7 V. Applying a stronger adsorption potential such as -0.1 V to TPA^+ on $DeACF_{10}$ vs. its OCP (+0.45 V) resulted in a significant improvement of q_m by 3.5 fold. In contrast, a slight reduction by 23% occurred under mild desorption (+0.6 V) compared to OCP condition. Interestingly, comparing the potential effects on q_m (**Table 2**) and log K_d (**Fig. 3**) for TPA^+ and *p*-TsO$^-$ where reversed potentials are needed to trigger ad- and desorption, the effect was lower for *p*-TsO$^-$ on both ACFs than for TPA$^+$. Even in the heaviest loaded case, TPA$^+$ on DeACF$_{10}$ at -0.1 V, pores larger than 1 nm were only filled to 25% (*Supporting Information*, **Table S4**). Thus, ACFs' pore volume should not limit the uptake of ionic PMOCs. Also noting that TPA$^+$ and *p*-TsO$^-$ show a similar value for log *D* (-0.45 and -0.17) [62], which implies similar hydrophobicity.

A recent study on electrosorption of the anionic form of aliphatic perfluorooctanoic acid (PFOA, pK_a < 1 [63], log *D* = 1.58 [62], carrying a strongly hydrophobic moiety) demonstrated a strong effect of AC charging on its sorption capacity (q_m differed by a factor of 9 over a 600 mV potential range) [15]. Thus, the as-observed much less sensitive potential effects on q_m of *p*-TsO$^-$ compared to TPA$^+$ could tentatively be related to a predominant, strong π-π electron donor-acceptor (π-π EDA) interaction between *p*-TsO$^-$ and ACF surfaces [64, 65] which maintain adsorption even under unfavorable electrostatic conditions. One needs to consider both entropic and enthalpic contributions to the adsorption equilibria resulting from various solute-solute and solute-surface interactions, including van-der-Waals, π-π, hydrogen bonding and electrostatic interactions. Electric polarization of the adsorbent can only cause exploitable effects on the PMOC sorption behavior when electrostatic interactions (attractive/repulsive) or charge-related effects (requirement of charge compensation for ionic adsorbates) significantly contribute to the free energy change in the adsorption processes.

3.3 Charging at bias potential vs. chemical modification of AC surface: Which has a stronger effect on PMOC adsorption?

The contribution of ACF surface modification on its electrosorption affinity to selected PMOCs can be visualized by referring *E* to E_{pzc} as shown in **Fig. 5**. When $E = E_{pzc}$, both DeACF$_{10}$ and

ACF_{10} surfaces carry zero net charge. The difference in log K_d at E (vs. E_{pzc}) = 0 indicates their different adsorption affinities towards a certain PMOC resulting from the intrinsically distinct sorbent surface chemistries. $DeACF_{10}$ generally showed higher adsorption affinities towards all three tested PMOCs at E (vs. E_{pzc}) = 0 due to its enhanced surface hydrophobicity, which strongly favors adsorption of PMOCs over water molecules and inorganic ions. As seen in **Fig. 5**, the difference in adsorption affinities of the two ACFs is not overcompensated by applying a potential bias in the studied potential ranges. However, strong modulating effects of potential on K_d were observed for the ionic PMOCs. For TPA^+ (**Fig. 5a**), cathodic charging of ACF_{10} is much more effective for increasing sorption affinity than surface chemical modifications where Freundlich parameters remained nearly unaffected by defunctionalization nor oxidation of the carbon surface [13] (**Figs. S10-11**, **Table S5**). Although surface defunctionalization improves the adsorbent hydrophobicity, it creates positively charged sites (by proton adsorption onto its delocalized π-electron systems) which repulse TPA^+ [13]. For p-TsO^- (**Fig. 5b**), comparable or stronger enhancement of ACF adsorption affinity can be caused by surface defunctionalization vs. anodic charging. A strong synergetic promotion effect on p-TsO^- adsorption was achieved on $DeACF_{10}$ surface carrying higher hydrophobicity and positive charges [13] (**Figs. S10-11, Table S5**). This suggests that an intrinsic alteration of the sorbent surface chemistry is required to achieve a remarkable interference in the adsorption behavior of p-TsO^- on ACFs predominated by π-π EDA interactions. AC surface charging can hardly manipulate its sorption affinity to nonionic *p*-TSA (**Fig. 5c**), whereas surface defunctionalization significantly improves it.

Even though AC's chemical or thermal surface modification can be applied to improve *ad*sorption performance, it is not applicable for initiating desorption in on-site regeneration as being practically irreversible. In contrast, surface charging via applying bias potential is switchable and can facilitate trap&release in continuous water treatment for PMOC removal.

3.4 System stability study

Experiments up to 5 adsorption-desorption cycles (48 h for each adsorption or desorption step) were performed to assess the system stability. As $DeACF_{10}$ delivers better electro-assisted trap&release performance than ACF_{10} (**Table 3**), we focused on the stability testing of electrosorption on $DeACF_{10}$. Especially, **Fig 5** indicates a strongly promoted adsorption of anionic PMOC at OCP for $DeACF_{10}$ whereas an effective desorption and in-situ adsorbent regeneration via cathodic polarization. Since nearly no effects of bias potentials were seen for nonionic *p*-TSA and MTBE, the long-term performance of electrosorption was exclusively tested for the two charged PMOC representatives TPA^+ and *p*-TsO^-. To obtain the optimal effects, we chose a potential of +0.6 V for the desorption and the adsorption conditions for TPA^+ and *p*-TsO^-, respectively (**Table 3**). Unlike -0.1 V chosen as the adsorption condition for TPA^+, desorption of *p*-TsO^- was probed under OCP as it shows almost the identical sorption isotherm with the one obtained at -0.1 V (**Fig. 4d**).

As shown in **Fig. 6**, $DeACF_{10}$ maintained a stable performance for electro-assisted trap&release of both TPA^+ and *p*-TsO^- over at least 5 cycles. There were only minor deviations of log K_d within its typical error range (±0.15 units).

We further recorded cyclic voltammograms and carried out TPD measurements (**Fig. 7**) to track the changes of the ACF electrodes after treatment under different electrosorption conditions. Since the cycled ACF samples were all washed and dried before characterization, a sample only washed and dried just like the cycled ACFs was characterized to serve as a reference (i.e., the sample ‘‘washed and dried’’). Despite the relatively insignificant changes in adsorption properties detected for most of the cycled DeACF$_{10}$ samples, a considerable alteration was found after using DeACF$_{10}$ for five cycles (at -0.1/+0.6 V) with the V-shape position shifted by +245 mV and the content of oxygen increased by 50% (**Table S6**). TPD shows CO_2 release with almost double the intensity compared to the ‘’washed and dried’’ DeACF$_{10}$ sample. This indicates the formation of more carboxylic, anhydride and/or lactone groups on the carbon surface [66, 67], also reflected by the changes in Raman spectra (**Fig. S13**). However, the corresponding pore size distribution, SSA and fiber morphology remained mostly unaffected (**Fig. S12, S14**). However, a ca. 20% sacrifice in total pore volume and SSA was caused when more harsh conditions (~-1 V vs. SHE) were applied to regenerate bentazone pre-loaded AC cloth over 6 cycles [18]. The minor alteration of DeACF$_{10}$ has not harmed the performance of DeACF$_{10}$ in electro-assisted trap&release of TPA$^+$ during the 5-cycle experiments, which is not surprising as TPA$^+$ adsorption was found adequate even on OxACF$_{10}$ surface of higher oxidation degree (**Fig. S10**, **Table S5**). The CV and TPD results reveal a more sensitive surface of ACF$_{10}$ upon charging, especially at a negative electric potential (**Fig. S15**). This seemingly implies a narrower range of applicable polarization conditions as suggested by cyclic voltammograms (Section 3.1, **Fig. 1**).

For simultaneous removal of anionic and cationic PMOCs from contaminated water in a trap&release electrosorption system, symmetric AC electrodes can be applied as anode and cathode covered with an anion- or cation-selective membrane, respectively, as also done in membrane CDI applications [21]. This setup should prevent re-adsorption of PMOCs released from one electrode to the other upon the potential switch in the desorption step.

4. Conclusions

In this work, electric polarization of ACF is demonstrated to substantially manipulate the ad- and desorption of charged PMOCs in aqueous media but has only a minor effect on nonionic PMOCs. Great potential is especially shown for electrosorptive removal of TPA^+ where charging ACF achieves large differences in adsorption affinities and capacities (factors of >50 in K_d and factors >5 in q_m). Smaller manipulating effects on *p*-TsO^- adsorption were proposed to be related to its strong π-π EDA interaction with ACF surfaces. Our study contributes to the development of currently non-existent prediction tools for the electrosorption performances of various PMOCs.

Cathodic polarization of AC offers an efficient way to enhance the *ad*sorption of cationic PMOCs, which is still challenging [68] and not achievable by surface oxidation as alternative approach to create negatively charged AC surfaces [13]. AC surface-defunctionalization increases the applicable potential window of ACF and fostered the trap&release performance even further. It also promotes adsorption of anionic contaminants with no need of anodic polarization. In addition, surface defunctionalization improves the adsorbent chemical stability, i.e. the usable potential window, and allows stronger hydrophobic effects. Significant system stability and high enrichment factors suggest a facile, green on-site regeneration alternative for exhausted ACFs through electro-assisted polarization.

Further research should employ flow-through systems to evaluate the potential of electro-assisted trap&release in treating real wastewaters. Nonetheless, our findings provide a guidance in AC-based materials modification and process design. The electrosorption techniques are able to effectively enrich PMOCs from large water flows in small water volumes. This can considerably lower the energy consumption of any further treatment technique such as electrochemical degradation [69, 70] to achieve the complete mineralization of PMOCs.

Acknowledgement

We are grateful for the funding offered by Deutsche Forschungsgemeinschaft GE 3029/1-1 and the PhD-college STROMER within the Thematic Area: Environmental Engineering and Biotechnology at UFZ. We thank Ms. Ruonan Qin for assisting the electrosorption experiments of MTBE in her internship and Dr. Navid Saeidi for fruitful discussions. The INM authors thank Prof. Dr. Eduard Arzt (INM) for his continuing support.

References

[1] All POPs listed in the Stockholm Convention. http://chm.pops.int/TheConvention/ThePOPs/AllPOPs/tabid/2509/Default.aspx. (Accessed 31 May 2021 2021).

[2] H.P.H. Arp, T.N. Brown, U. Berger, S.E. Hale, Ranking REACH registered neutral, ionizable and ionic organic chemicals based on their aquatic persistency and mobility, Environ. Sci.: Process. Impacts. 19(7) (2017) 939-955. https://doi.org/https://doi.org/10.1039/C7EM00158D.

[3] R. Loos, R. Carvalho, D.C. António, S. Comero, G. Locoro, S. Tavazzi, B. Paracchini, M. Ghiani, T. Lettieri, L. Blaha, B. Jarosova, S. Voorspoels, K. Servaes, P. Haglund, J. Fick, R.H. Lindberg, D. Schwesig, B.M. Gawlik, EU-wide monitoring survey on emerging polar organic contaminants in wastewater treatment plant effluents, Water Res. 47(17) (2013) 6475-6487. https://doi.org/https://doi.org/10.1016/j.watres.2013.08.024.

[4] T. Reemtsma, U. Berger, H.P.H. Arp, H. Gallard, T.P. Knepper, M. Neumann, J.B. Quintana, P.d. Voogt, Mind the gap: persistent and mobile organic compounds—water contaminants that slip through, Environ. Sci. Technol. 50(19) (2016) 10308-10315. https://doi.org/https://doi.org/10.1021/acs.est.6b03338.

[5] S.E. Hale, H.P.H. Arp, I. Schliebner, M. Neumann, Persistent, mobile and toxic (PMT) and very persistent and very mobile (vPvM) substances pose an equivalent level of concern to persistent, bioaccumulative and toxic (PBT) and very persistent and very bioaccumulative (vPvB) substances under REACH, Environ. Sci. Eur. 32(1) (2020) 155. https://doi.org/https://doi.org/10.1186/s12302-020-00440-4.

[6] C. Sophia A, E.C. Lima, Removal of emerging contaminants from the environment by adsorption, Ecotoxicol. Environ. Saf. 150 (2018) 1-17. https://doi.org/https://doi.org/10.1016/j.ecoenv.2017.12.026.

[7] M. Bonato, F. Corrà, M. Bellio, L. Guidolin, L. Tallandini, P. Irato, G. Santovito, PFAS environmental pollution and antioxidant responses: An overview of the impact on human field, Int. J. Environ. Res. Public Health 17(21) (2020). https://doi.org/https://doi.org/10.3390/ijerph17218020.

[8] P. Roslev, T. Lentz, M. Hesselsoe, Microbial toxicity of methyl tert-butyl ether (MTBE) determined with fluorescent and luminescent bioassays, Chemosphere 120 (2015) 284-291. https://doi.org/https://doi.org/10.1016/j.chemosphere.2014.07.003.

[9] S. Schulze, D. Zahn, R. Montes, R. Rodil, J.B. Quintana, T.P. Knepper, T. Reemtsma, U. Berger, Occurrence of emerging persistent and mobile organic contaminants in European water samples, Water Res. 153 (2019) 80-90. https://doi.org/https://doi.org/10.1016/j.watres.2019.01.008.

[10] L. Decrey, F. Bonvin, C. Bonvin, E. Bonvin, T. Kohn, Removal of trace organic contaminants from wastewater by superfine powdered activated carbon (SPAC) is neither affected by SPAC dispersal nor coagulation, Water Res. 185 (2020) 116302. https://doi.org/https://doi.org/10.1016/j.watres.2020.116302.

[11] N. Saeidi, F.-D. Kopinke, A. Georgi, Understanding the effect of carbon surface chemistry on adsorption of perfluorinated alkyl substances, Chem. Eng. J. 381 (2020) 122689. https://doi.org/https://doi.org/10.1016/j.cej.2019.122689.

[12] N. Saeidi, F.-D. Kopinke, A. Georgi, What is specific in adsorption of perfluoroalkyl acids on carbon materials?, Chemosphere (2020) 128520. https://doi.org/https://doi.org/10.1016/j.chemosphere.2020.128520.

[13] J. Zhou, N. Saeidi, L.Y. Wick, F.-D. Kopinke, A. Georgi, Adsorption of polar and ionic organic compounds on activated carbon: surface chemistry matters, Sci. Total Environ. (2021) 148508. https://doi.org/https://doi.org/10.1016/j.scitotenv.2021.148508.

[14] L. Li, P.A. Quinlivan, D.R.U. Knappe, Effects of activated carbon surface chemistry and pore structure on the adsorption of organic contaminants from aqueous solution, Carbon 40(12) (2002) 2085-2100. https://doi.org/https://doi.org/10.1016/S0008-6223(02)00069-6.

[15] N. Saeidi, F.-D. Kopinke, A. Georgi, Controlling adsorption of perfluoroalkyl acids on activated carbon felt by means of electrical potentials, Chem. Eng. J. 416 (2021) 129070. https://doi.org/https://doi.org/10.1016/j.cej.2021.129070.

[16] E. Bayram, E. Ayranci, Electrochemically enhanced removal of polycyclic aromatic basic dyes from dilute aqueous solutions by activated carbon cloth electrodes, Environ. Sci. Technol. 44(16) (2010) 6331-6336. https://doi.org/https://doi.org/10.1021/es101177k.

[17] E. Bayram, E. Ayranci, Structural effects on electrosorptive behavior of aromatic organic acids from aqueous solutions onto activated carbon cloth electrode of a flow-through electrolytic cell, J. Electroanal. Chem. 683 (2012) 14-20. https://doi.org/https://doi.org/10.1016/j.jelechem.2012.07.028.

[18] C.O. Ania, F. Béguin, Electrochemical regeneration of activated carbon cloth exhausted with bentazone, Environ. Sci. Technol. 42(12) (2008) 4500-4506. https://doi.org/https://doi.org/10.1021/es703192x.

[19] S. Delpeux-Ouldriane, M. Gineys, N. Cohaut, F. Béguin, The role played by local pH and pore size distribution in the electrochemical regeneration of carbon fabrics loaded with bentazon, Carbon 94 (2015) 816-825. https://doi.org/https://doi.org/10.1016/j.carbon.2015.07.010.

[20] E. Gagliano, M. Sgroi, P.P. Falciglia, F.G.A. Vagliasindi, P. Roccaro, Removal of poly- and perfluoroalkyl substances (PFAS) from water by adsorption: Role of PFAS chain length, effect of organic matter and challenges in adsorbent regeneration, Water Res. 171 (2020) 115381. https://doi.org/https://doi.org/10.1016/j.watres.2019.115381.

[21] M.E. Suss, S. Porada, X. Sun, P.M. Biesheuvel, J. Yoon, V. Presser, Water desalination via capacitive deionization: what is it and what can we expect from it?, Energy Environ. Sci. 8(8) (2015) 2296-2319. https://doi.org/https://doi.org/10.1039/C5EE00519A.

[22] L. Wang, Y. Zhang, K. Moh, V. Presser, From capacitive deionization to desalination batteries and desalination fuel cells, Curr. Opin. Electrochem. (2021) 100758. https://doi.org/https://doi.org/10.1016/j.coelec.2021.100758.

[23] Y. Han, X. Quan, H. Zhao, S. Chen, Y. Zhao, Kinetics of enhanced adsorption by polarization for organic pollutants on activated carbon fiber, Front. Environ. Sci. Eng. China 1(1) (2007) 83-88. https://doi.org/https://doi.org/10.1007/s11783-007-0016-2.

[24] C.O. Ania, F. Béguin, Mechanism of adsorption and electrosorption of bentazone on activated carbon cloth in aqueous solutions, Water Res. 41(15) (2007) 3372-3380. https://doi.org/https://doi.org/10.1016/j.watres.2007.03.031.

[25] O. Kitous, A. Cheikh, H. Lounici, H. Grib, A. Pauss, N. Mameri, Application of the electrosorption technique to remove Metribuzin pesticide, J. Hazard. Mater. 161(2) (2009) 1035-1039. https://doi.org/https://doi.org/10.1016/j.jhazmat.2008.04.091.

[26] W. Yang, H. Han, M. Zhou, J. Yang, Simultaneous electricity generation and tetracycline removal in continuous flow electrosorption driven by microbial fuel cells, RSC Adv. 5(61) (2015) 49513-49520. https://doi.org/https://doi.org/10.1039/C5RA05545H.

[27] S. López-Bernabeu, R. Ruiz-Rosas, C. Quijada, F. Montilla, E. Morallón, Enhanced removal of 8-quinolinecarboxylic acid in an activated carbon cloth by electroadsorption in

aqueous solution, Chemosphere 144 (2016) 982-988. https://doi.org/https://doi.org/10.1016/j.chemosphere.2015.09.071.

[28] E. Bayram, Ç. Kızıl, E. Ayrancı, Flow-through electrosorption process for removal of 2,4-D pesticide from aqueous solutions onto activated carbon cloth fixed-bed electrodes, Water Sci. Technol. 77(3) (2018) 848-854. https://doi.org/https://doi.org/10.2166/wst.2017.598.

[29] S. Wang, X. Li, H. Zhao, X. Quan, S. Chen, H. Yu, Enhanced adsorption of ionizable antibiotics on activated carbon fiber under electrochemical assistance in continuous-flow modes, Water Res. 134 (2018) 162-169. https://doi.org/https://doi.org/10.1016/j.watres.2018.01.068.

[30] X. Li, Y. Hu, D. She, W.-B. Shen, Modified activated carbon fiber felt for the electrosorption of norfloxacin in aqueous solution, Sustainability 12(10) (2020). https://doi.org/https://doi.org/10.3390/su12103986.

[31] Y. Lester, E. Shaulsky, R. Epsztein, I. Zucker, Capacitive deionization for simultaneous removal of salt and uncharged organic contaminants from water, Sep. Purif. Technol. 237 (2020) 116388. https://doi.org/https://doi.org/10.1016/j.seppur.2019.116388.

[32] J. Niu, B.E. Conway, Adsorptive and electrosorptive removal of aniline and bipyridyls from waste-waters, J. Electroanal. Chem. 536(1) (2002) 83-92. https://doi.org/https://doi.org/10.1016/S0022-0728(02)01206-8.

[33] J. Niu, B.E. Conway, Molecular structure factors in adsorptive removal of pyridinium cations, 1,4-pyrazine and 1-quinoline at high-area C-cloth electrodes for waste-water remediation, J. Electroanal. Chem. 529(2) (2002) 84-96. https://doi.org/https://doi.org/10.1016/S0022-0728(02)00910-5.

[34] J.M. Serrano, A.U. Khan, T. Liu, Z. Xu, A.R. Esker, G. Liu, Capacitive organic dye removal by block copolymer based porous carbon fibers, Adv. Mater. Interfaces 7(16) (2020) 2000507. https://doi.org/https://doi.org/10.1002/admi.202000507.

[35] E. Ayranci, B.E. Conway, Adsorption and electrosorption of ethyl xanthate and thiocyanate anions at high-area carbon-cloth electrodes studied by in situ UV spectroscopy: Development of procedures for wastewater purification, Anal. Chem. 73(6) (2001) 1181-1189. https://doi.org/https://doi.org/10.1021/ac000736e.

[36] F.E. Woodard, D.E. McMackins, R.E.W. Jansson, Electrosorption of organics on three dimensional carbon fiber electrodes, J. Electroanal. Chem. Interf. Electrochem. 214(1) (1986) 303-330. https://doi.org/https://doi.org/10.1016/0022-0728(86)80105-X.

[37] A. Ban, A. Schafer, H. Wendt, Fundamentals of electrosorption on activated carbon for wastewater treatment of industrial effluents, J. Appl. Electrochem. 28(3) (1998) 227-236. https://doi.org/https://doi.org/10.1023/A:1003247229049.

[38] E. Bayram, E. Ayranci, Investigation of changes in properties of activated carbon cloth upon polarization and of electrosorption of the dye basic blue-7, Carbon 48(6) (2010) 1718-1730. https://doi.org/https://doi.org/10.1016/j.carbon.2010.01.013.

[39] J.P. Guthrie, Hydrolysis of esters of oxy acids: pKa values for strong acids; Brønsted relationship for attack of water at methyl; free energies of hydrolysis of esters of oxy acids; and a linear relationship between free energy of hydrolysis and pKa holding over a range of 20 pK units, Can. J. Chem. 56(17) (1978) 2342-2354. https://doi.org/https://doi.org/10.1139/v78-385.

[40] E.P. Sergeant, B. Dempsey, Ionisation constants of organic acids in aqueous solution. IUPAC chemical data series No. 23, Pergamon Press, New York, 1979.

[41] J.L. Atwood, J.W. Steed, Encyclopedia of supramolecular chemistry CRC Press, New York, 2004. https://doi.org/https://doi.org/10.1201/9780429075728

[42] S. Schulze, D. Sättler, M. Neumann, H.P.H. Arp, T. Reemtsma, U. Berger, Using REACH registration data to rank the environmental emission potential of persistent and mobile organic chemicals, Sci. Total Environ. 625 (2018) 1122-1128. https://doi.org/https://doi.org/10.1016/j.scitotenv.2017.12.305.

[43] D. Richter, U. Dünnbier, G. Massmann, A. Pekdeger, Quantitative determination of three sulfonamides in environmental water samples using liquid chromatography coupled to electrospray tandem mass spectrometry, J. Chromatogr. A 1157(1) (2007) 115-121. https://doi.org/https://doi.org/10.1016/j.chroma.2007.04.042.

[44] A. Kolkman, D. Vughs, R. Sjerps, P.J.F. Kooij, M. van der Kooi, K. Baken, J. Louisse, P. de Voogt, Assessment of highly polar chemicals in Dutch and Flemish drinking water and its sources: presence and potential risks, ACS ES&T Water 1(4) (2021) 928-937. https://doi.org/10.1021/acsestwater.0c00237.

[45] E.R. Mancini, A. Steen, G.A. Rausina, D.C.L. Wong, W.R. Arnold, F.E. Gostomski, T. Davies, J.R. Hockett, W.A. Stubblefield, K.R. Drottar, T.A. Springer, P. Errico, MTBE ambient water quality criteria development: a public/private partnership, Environ. Sci. Technol. 36(2) (2002) 125-129. https://doi.org/10.1021/es002059b.

[46] B.M. Babić, S.K. Milonjić, M.J. Polovina, B.V. Kaludierović, Point of zero charge and intrinsic equilibrium constants of activated carbon cloth, Carbon 37(3) (1999) 477-481. https://doi.org/https://doi.org/10.1016/S0008-6223(98)00216-4.

[47] D. Weingarth, M. Zeiger, N. Jäckel, M. Aslan, G. Feng, V. Presser, Graphitization as a universal tool to tailor the potential-dependent capacitance of carbon supercapacitors, Adv.

Energy Mater. 4(13) (2014) 1400316. https://doi.org/https://doi.org/10.1002/aenm.201400316.

[48] L.-H. Shao, J. Biener, D. Kramer, R.N. Viswanath, T.F. Baumann, A.V. Hamza, J. Weissmüller, Electrocapillary maximum and potential of zero charge of carbon aerogel, Phys. Chem. Chem. Phys. 12(27) (2010) 7580-7587. https://doi.org/https://doi.org/10.1039/B916331J.

[49] V. Lockett, R. Sedev, J. Ralston, M. Horne, T. Rodopoulos, Differential Capacitance of the Electrical Double Layer in Imidazolium-Based Ionic Liquids: Influence of Potential, Cation Size, and Temperature, J. Phys. Chem. C 112(19) (2008) 7486-7495. https://doi.org/https://doi.org/10.1021/jp7100732.

[50] C. Zhang, D. He, J. Ma, W. Tang, T.D. Waite, Faradaic reactions in capacitive deionization (CDI) - problems and possibilities: A review, Water Res. 128 (2018) 314-330. https://doi.org/https://doi.org/10.1016/j.watres.2017.10.024.

[51] N. Holubowitch, A. Omosebi, X. Gao, J. Landon, K. Liu, Quasi-steady-state polarization reveals the interplay of capacitive and Faradaic processes in capacitive deionization, ChemElectroChem 4(9) (2017) 2404-2413. https://doi.org/https://doi.org/10.1002/celc.201700082.

[52] E. Bayram, E. Ayranci, A systematic study on the changes in properties of an activated carbon cloth upon polarization, Electrochim. Acta 56(5) (2011) 2184-2189. https://doi.org/https://doi.org/10.1016/j.electacta.2010.12.018.

[53] G. Hotová, V. Slovák, T. Zelenka, R. Maršálek, A. Parchaňská, The role of the oxygen functional groups in adsorption of copper (II) on carbon surface, Sci. Total Environ. 711 (2020) 135436. https://doi.org/https://doi.org/10.1016/j.scitotenv.2019.135436.

[54] X. Gao, A. Omosebi, J. Landon, K. Liu, Surface charge enhanced carbon electrodes for stable and efficient capacitive deionization using inverted adsorption–desorption behavior, Energy Environ. Sci. 8(3) (2015) 897-909. https://doi.org/https://doi.org/10.1039/C4EE03172E.

[55] C.-H. Hou, C. Liang, S. Yiacoumi, S. Dai, C. Tsouris, Electrosorption capacitance of nanostructured carbon-based materials, J. Colloid Interface Sci. 302(1) (2006) 54-61. https://doi.org/https://doi.org/10.1016/j.jcis.2006.06.009.

[56] A. Lasia, Electrochemical impedance spectroscopy and its applications. In: Conway B.E., Bockris J.O., White R.E. (eds) Modern aspects of electrochemistry. Modern aspects of electrochemistry, Springer, Boston, MA, 2002. https://doi.org/https://doi.org/10.1007/0-306-46916-2_2.

[57] T. Bordjiba, M. Mohamedi, L.H. Dao, Synthesis and electrochemical capacitance of binderless nanocomposite electrodes formed by dispersion of carbon nanotubes and carbon aerogels, J. Power Sources 172(2) (2007) 991-998. https://doi.org/https://doi.org/10.1016/j.jpowsour.2007.05.011.

[58] D.D. Macdonald, Reflections on the history of electrochemical impedance spectroscopy, Electrochim. Acta 51(8) (2006) 1376-1388. https://doi.org/https://doi.org/10.1016/j.electacta.2005.02.107.

[59] J. Lybaert, B.U.W. Maes, K. Abbaspour Tehrani, K. De Wael, The electrochemistry of tetrapropylammonium perruthenate, its role in the oxidation of primary alcohols and its potential for electrochemical recycling, Electrochim. Acta 182 (2015) 693-698. https://doi.org/https://doi.org/10.1016/j.electacta.2015.09.107.

[60] C.K. Mann, P.T. Cottrell, Electrochemical reduction of arylsulfonamides, J. Am. Chem. Soc. 93(15) (1971) 3579-3583. https://doi.org/http://doi.org/10.1021/ja00744a006.

[61] T.D. Appleman, C.P. Higgins, O. Quiñones, B.J. Vanderford, C. Kolstad, J.C. Zeigler-Holady, E.R.V. Dickenson, Treatment of poly- and perfluoroalkyl substances in U.S. full-scale water treatment systems, Water Res. 51 (2014) 246-255. https://doi.org/https://doi.org/10.1016/j.watres.2013.10.067.

[62] ChemAxon online platform, https://chemicalize.com. (Accessed 11 June 2021).

[63] K.-U. Goss, The pKa values of PFOA and other highly fluorinated carboxylic acids, Environ. Sci. Technol. 42(2) (2008) 456-458. https://doi.org/https://doi.org/10.1021/es702192c.

[64] X.-F. Sun, B.-B. Guo, L. He, P.-F. Xia, S.-G. Wang, Electrically accelerated removal of organic pollutants by a three-dimensional graphene aerogel, AIChE Journal 62(6) (2016) 2154-2162. https://doi.org/https://doi.org/10.1002/aic.15185.

[65] D. Zhu, J.J. Pignatello, Characterization of aromatic compound sorptive interactions with black carbon (charcoal) assisted by graphite as a model, Environ. Sci. Technol. 39(7) (2005) 2033-2041. https://doi.org/http://doi.org/10.1021/es0491376.

[66] M. Vogel, F.-D. Kopinke, K. Mackenzie, Acceleration of microiron-based dechlorination in water by contact with fibrous activated carbon, Sci. Total Environ. 660 (2019) 1274-1282. https://doi.org/https://doi.org/10.1016/j.scitotenv.2019.01.070.

[67] J.-H. Zhou, Z.-J. Sui, J. Zhu, P. Li, D. Chen, Y.-C. Dai, W.-K. Yuan, Characterization of surface oxygen complexes on carbon nanofibers by TPD, XPS and FT-IR, Carbon 45(4) (2007) 785-796. https://doi.org/https://doi.org/10.1016/j.carbon.2006.11.019.

[68] G. Sigmund, M. Gharasoo, T. Hüffer, T. Hofmann, Deep learning neural network approach for predicting the sorption of ionizable and polar organic pollutants to a wide range of carbonaceous materials, Environ. Sci. Technol. 54(7) (2020) 4583–4591. https://doi.org/http://doi.org/10.1021/acs.est.9b06287.

[69] Y. Chen, Y. Tu, Y. Bai, J. Li, J. Lu, Electrosorption enhanced electrooxidation of a model organic pollutant at 3D SnO2-Sb electrode in superimposed pulse current mode, Chemosphere 195 (2018) 63-69. https://doi.org/https://doi.org/10.1016/j.chemosphere.2017.12.074.

[70] K. Kim, P. Baldaguez Medina, J. Elbert, E. Kayiwa, R.D. Cusick, Y. Men, X. Su, Molecular tuning of redox-copolymers for selective electrochemical remediation, Adv. Funct. Mater. 30(52) (2020) 2004635. https://doi.org/https://doi.org/10.1002/adfm.202004635.

Figures

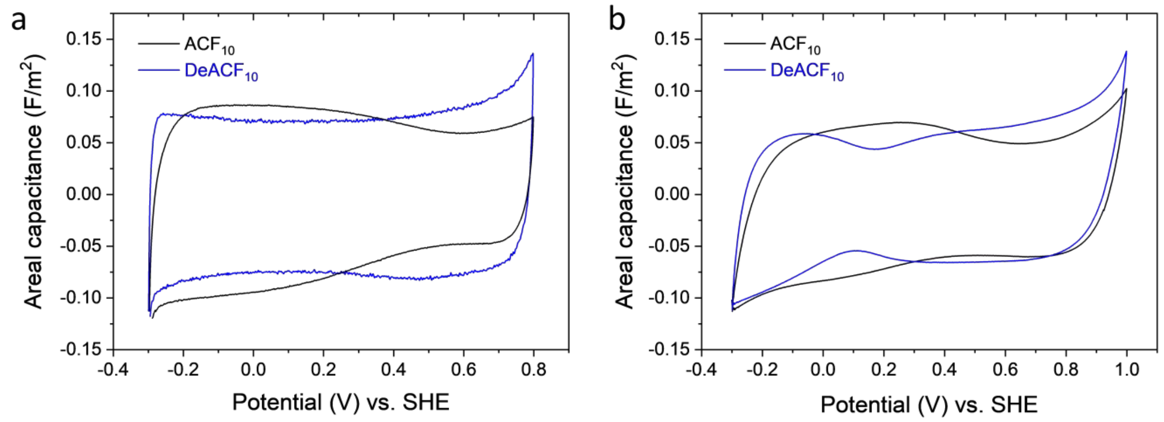

Figure 1: Cyclic voltammograms of ACF_{10} and $DeACF_{10}$ (a) in 1 M Na_2SO_4 at 1 mV/s and (b) in 10 mM Na_2SO_4 at 0.5 mV/s.

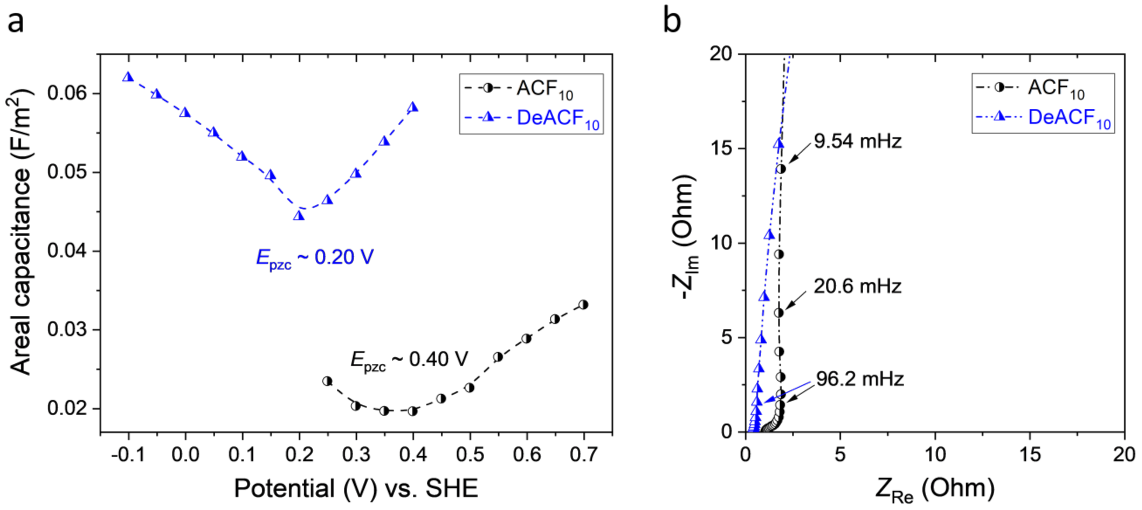

Figure 2: (a) Areal capacitance of ACFs at various applied potentials measured at 96.2 mHz. (b) Nyquist plots of ACFs polarized at 0.4 V vs. SHE. Lines serve as guides for the eye.

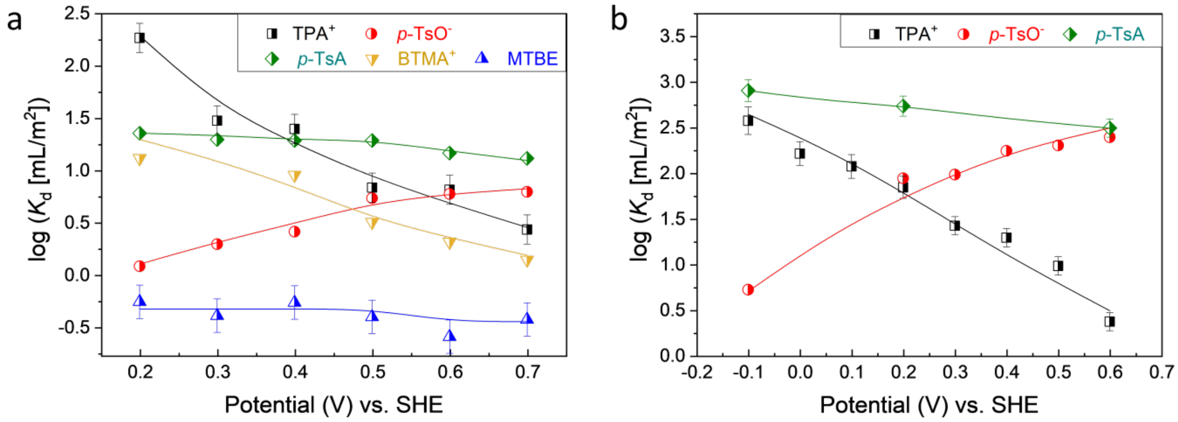

Figure 3: Log K_d of selected PMOCs on polarized (a) ACF$_{10}$ and (b) DeACF$_{10}$. Initial solute concentration: 20 mg/L; ACF dosage: 1 g/L. The error bars indicate the typical deviation of single values from the mean for duplicate experiments. Lines serve as guides for the eye.

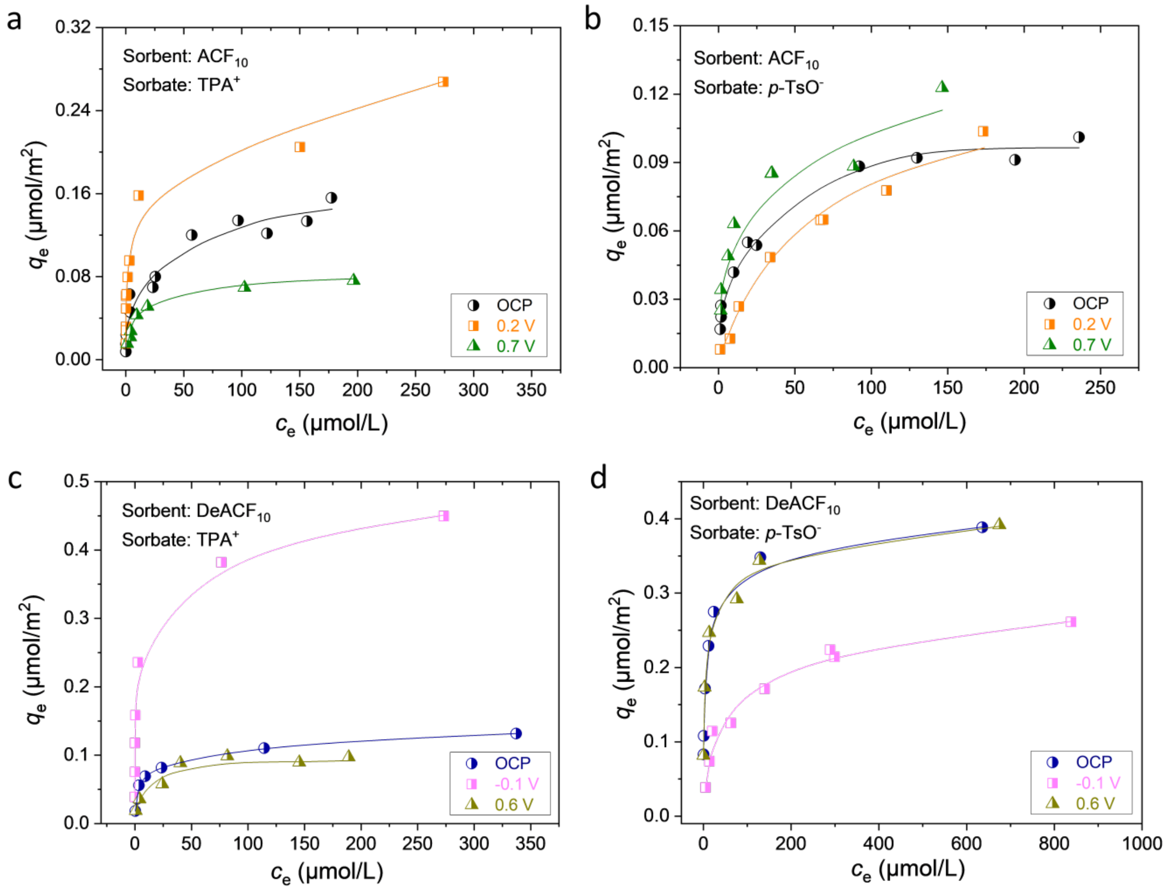

Figure 4: Adsorption isotherms obtained at different potentials. OCPs of ACF$_{10}$ and DeACF$_{10}$ are around 0.45 V. All potential values are given vs. SHE. Lines serve as guides for the eye. Langmuir and Freundlich linear fittings are shown in *Supporting Information*, **Fig. S5-S6**.

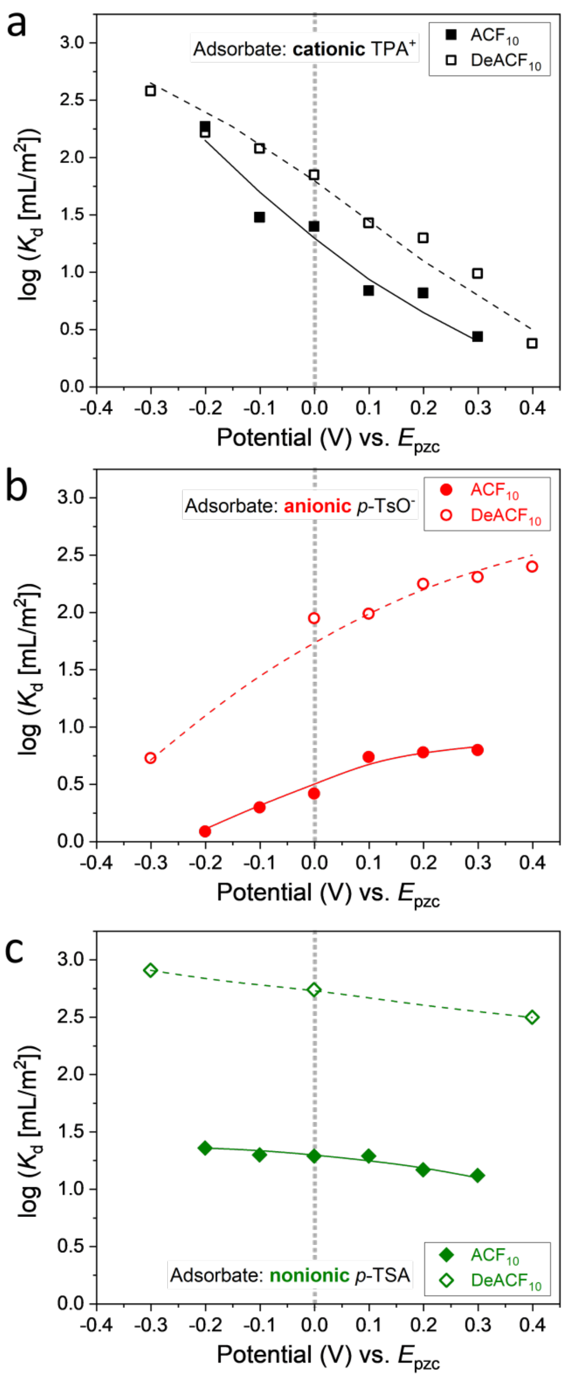

Figure 5: Log K_d of selected PMOCs on polarized ACF$_{10}$ (filled symbols) and DeACF$_{10}$ (hollow symbols). The applied potential is referred to E_{pzc} in the x-axis. The E_{pzc} of ACF$_{10}$ and DeACF$_{10}$ are ca. 0.4 V and 0.2 V vs. SHE, respectively. Initial solute concentration: 20 mg/L; ACF dosage: 1 g/L. Lines serve as guides for the eye.

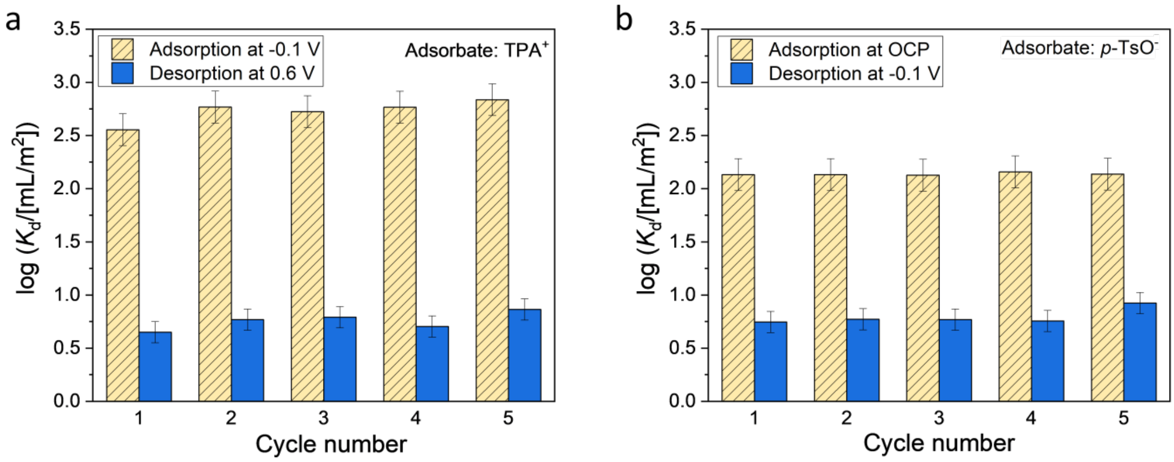

Figure 6: Log K_d of (a) TPA^+ and (b) *p*-TsO^- on $DeACF_{10}$ over 5 electro-assisted adsorption and desorption cycles. Initial solute concentration: 20 mg/L; ACF dosage: 1 g/L. All potential values are given vs. SHE. The error bars indicate the typical deviation of single values from the mean for duplicate experiments. Lines serve as guides for the eye.

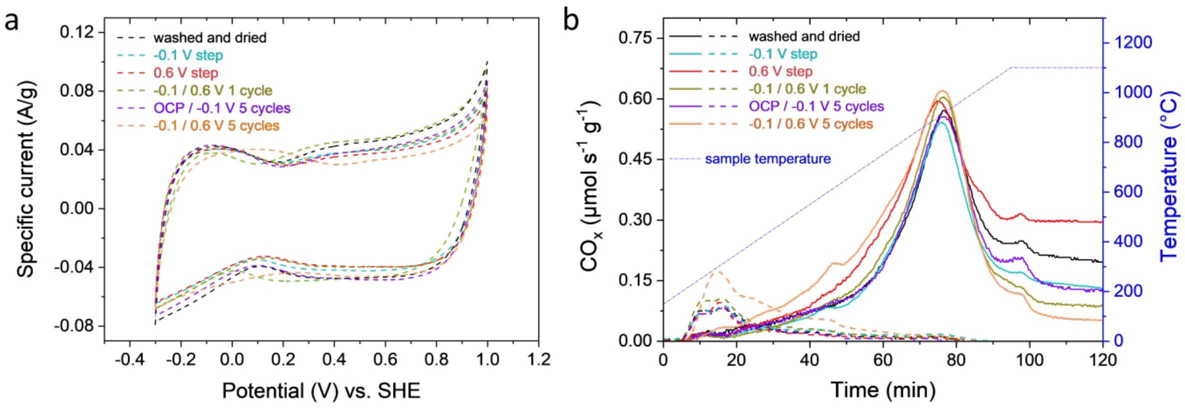

Figure 7: (a) Cyclic voltammograms and (b) TPD measurements of DeACF$_{10}$ after treating under different conditions. CV was performed in 10 mM Na_2SO_4 at 0.5 mV/s. In (b), solid and dashed lines represent the CO and CO_2 release profiles, respectively. All potential values are given vs. SHE.

Tables

Table 1: Selected properties of studied PMOCs. References given in brackets.

	TPA^+	**$BTMA^+$**	***p*-TsOH**	***p*-TSA**	**MTBE**
Type^a	cationic	cationic	anionic	nonionic	nonionic
pK_a	-	-	-1.3 [40]	10.5 [41]	-
log D^b	-0.45	-2.25	-0.71	1.09	1.18
Mol. weight (g/mol)	186.4	150.2	172.2	171.22	88.15
Structure	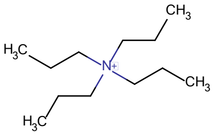	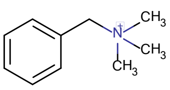	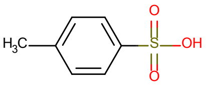	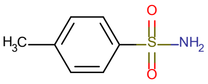	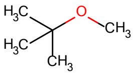

^{a} Predominant form at pH = 7. ^{b} Log D is the pH-dependent octanol-water distribution coefficient, obtained from [62] at pH 7. For MTBE (not ionizable), log D = pH-independent log K_{OW}.

Table 2: Freundlich and Langmuir isotherm fitting parameters for electrosorption of TPA$^+$ and *p*-TsO$^-$ on ACFs.

Sorbate	**Sorbent**	**Conditions (V) vs. SHE**	**Freundlich**			**Langmuir**		
			K_F ([µmol/m^2]/[µmol/L]^n)	n	R^2	q_m (µmol/m^2)	K_L (L/µmol)	R^2
TPA$^+$	ACF$_{10}$	0.45 (at OCP)	0.031 ± 0.006	0.44 ± 0.04	0.970	0.15 ± 0.01	0.11 ± 0.09	0.974
		0.20 (Ads.)	0.072 ± 0.007	0.33 ± 0.02	0.978	0.25 ± 0.02	0.26 ± 0.14	0.983
		0.70 (Des.)	0.014 ± 0.002	0.47 ± 0.05	0.962	0.078 ± 0.002	0.12 ± 0.03	0.999
	DeACF$_{10}$	0.45 (at OCP)	0.029 ± 0.004	0.43 ± 0.05	0.977	0.13 ± 0.01	0.11 ± 0.09	0.996
		-0.10 (Ads.)	0.20 ± 0.06	0.30 ± 0.04	0.955	0.45 ± 0.01	0.44 ± 0.23	0.998
		0.60 (Des.)	0.020 ± 0.003	0.37 ± 0.04	0.978	0.10 ± 0.01	0.18 ± 0.10	0.992
p-TsO$^-$	ACF$_{10}$	0.45 (at OCP)	0.017 ± 0.002	0.38 ± 0.02	0.988	0.10 ± 0.01	0.084 ± 0.036	0.993
		0.20 (Des.)	0.0037 ± 0.0013	0.69 ± 0.09	0.956	0.090 ± 0.010	0.042 ± 0.022	0.964
		0.70 (Ads.)	0.024 ± 0.003	0.38 ± 0.03	0.976	0.12 ± 0.01	0.13 ± 0.07	0.962
	DeACF$_{10}$	0.45 (at OCP)	0.110 ± 0.005	0.31 ± 0.01	0.994	0.39 ± 0.01	0.14 ± 0.08	1.000
		-0.10 (Des.)	0.021 ± 0.003	0.44 ± 0.04	0.980	0.27 ± 0.01	0.018 ± 0.006	0.993
		0.60 (Ads.)	0.12 ± 0.02	0.23 ± 0.03	0.950	0.41 ± 0.01	0.09 ± 0.04	0.999

Table 3: Electro-assisted trap&release parameters and performances for TPA^+ and *p*-TsO^- adsorption on ACFs under fixed-bed flow-through conditions estimated according to **Eqs. 4-7**.

		Bias potential (V) vs. SHE		**Enrichment factors**	
Sorbate	**Sorbent**	**Trap step**	**Release step**	V_{ads}/V_{des}[a]	V_{ads}/V_{des}[b]
TPA^+	ACF_{10}	0.2	0.7	74.2 (0.86)	64.7
	$DeACF_{10}$	-0.1	0.6	851 (0.91)	780
p-TsO^-	ACF_{10}	0.7	0.2	44.7 (0.92)	42.3
	$DeACF_{10}$	0.6	-0.1	176 (0.89)	158

[a] Using inflow water (water to be treated) for desorption. X_{des} given in brackets. [b] Using clean water for desorption, that is, X_{des} = 1.